This is a preprint of an article accepted for publication in ASCE Journal of Bridge Engineering on 19 September 2012. The published article is available online at http://ascelibrary.org/doi/abs/10.1061/(ASCE)BE.1943-5592.0000442

To be cited as: Wei K., Yuan W., Bouaanani N. 2013. Experimental and numerical assessment of the three dimensional modal dynamic response of bridge pile foundations submerged in water. ASCE Journal of Bridge Engineering, 18(10): 1032–1041.

Experimental and numerical assessment of the three-dimensional modal dynamic response of bridge pile foundations submerged in water

Kai Wei, S.M.ASCE [1]; Wancheng Yuan, A.M.ASCE [2]; Najib Bouaanani, M.ASCE [3]

Abstract: This paper describes an experimental program conducted to investigate the effects of fluid-structure interaction on the modal dynamic response of three reduced-scale bridge pile foundations submerged partially or totally in water. The vibration periods of the specimens are measured for the two lateral modes and first torsional mode using ambient and forced-vibration tests. The results are presented and discussed as a function of surrounding water levels and the number and geometrical patterns of the piles. Three-dimensional (3D) finite element models of the tested specimens surrounded by different water levels are built and the results are successfully validated against the obtained experimental data. The built numerical models are used to compute 3D modal hydrodynamic pressures. A systematic analysis of the period ratios and 3D hydrodynamic loads is presented to characterize the effects of pile cap, water height and the number and geometrical pattern of the piles on dynamic response. The experimental and numerical results of this research allow a better understanding of the complex dynamically-induced fluid-structure interaction effects in the response of deep water bridge pile foundations.

CE Database subject headings: Bridge; Pile foundations; Deep water; 3D analysis; Modal dynamic analysis; Finite elements; Fluid-structure interaction; Hydrodynamics; Pile groups; Pile caps.

[1] Ph.D. Candidate, State Key Laboratory of Disaster Reduction in Civil Engineering, Tongji University, Shanghai 200092, China; and Visiting Researcher, Department of Civil, Geological and Mining Engineering, École Polytechnique de Montréal, Montréal, QC H3C 3A7, Canada. E-mail: kai.wei@polymtl.ca

[2] Professor, State Key Laboratory of Disaster Reduction in Civil Engineering, Tongji University, Shanghai 200092, China. Corresponding author. E-mail: yuan@tongji.edu.cn

[3] Professor, Department of Civil, Geological and Mining Engineering, École Polytechnique de Montréal, Montréal, QC H3C 3A7, Canada. E-mail: najib.bouaanani@polymtl.ca

Introduction

Deep water bridges are popular solutions for crossing large spans of rivers, straits or portions of oceans (Feng 2009). In recent years, pile foundations have been widely used in deep water long-span bridges due to their structural efficiency, low cost and ease of construction (Ingham et al. 1999; DiMaggio and Goble 2004; AbdelSalam et al. 2010). Such bridge foundations, as those of Sutong Bridge (Bittner et al. 2007), China East Sea Bridge (Liu et al. 2007) and Xiangshan Bridge (Gao et al. 2008), consist mainly of a group of long piles extending to the soil below water surface and connected through a large concrete cap. In addition to the piles, most of these foundations have their pile caps partially or totally submerged in the water, thus contributing to the induced dynamic fluid-structure interaction effects. Long span deep water bridges need to be designed to withstand various dynamic loads such as those arising from traffic, earthquakes or winds (Virola 2005; You et al. 2008). One of the key factors when considering this type of loads is fluid-structure interaction between the vibrating bridge pile foundation and the surrounding water. Previous research on civil engineering structures showed that fluid-structure interaction during earthquakes might indeed alter the dynamic properties of the structural system and lead to additional hydrodynamic loads (Liaw and Chopra 1974; Uściłowska and Kołodziej 1998; Öz 2003; Zhang 2006; Wei et al. 2011). Several analytical approaches have been proposed to solve fluid-structure interaction problems involving cylindrical structures, e.g. piles or towers, submerged in water (Morison et al. 1950; Liaw and Chopra 1973; Bhatta and Rahman 2003). Numerical methods based on either finite elements or boundary elements have also been proposed to overcome the limitations of the analytical procedures (Everstine 1981; Olson and Bathe 1985; Zhang 2001; Di Pilato et al. 2008; Bouaanani and Lu 2009).

The dynamic response of a deep water bridge subjected to earthquake excitation depends on the dominant period of the seismic input and the vibration periods of the bridge-foundation-water system along various modes. In this regard, modal dynamic analysis is an effective and common tool that can be used to obtain dynamic characteristics of vibrating structures. Most of the previous studies in this field however focused on single cylindrical piles submerged in water, and the modal dynamic behavior of bridge foundations made of grouped piles was rarely investigated, especially when the pile cap is also surrounded partially or totally by water. An extensive literature review also highlighted the scarcity of published experimental work to validate the numerical procedures used to investigate the modal dynamic behavior of bridge pile foundations submerged in water and better understand the dynamically-induced fluid-structure interaction effects.

Objectives and Scope

The main purpose of this work is to assess the modal dynamic response of bridge foundation piles surrounded by water. Accordingly, the following objectives are set : (i) to conduct an experimental program to investigate the effects of fluid-structure interaction on the modal dynamic response of three reduced-scale bridge pile foundations and discuss the obtained results as a function of surrounding water levels and the number and geometrical patterns of the piles, (ii) to build three-dimensional (3D) finite element models of the tested specimens including fluid-structure interaction effects and validate the results against

dry and coupled vibration periods obtained from experimental data, and (iii) to use the validated numerical models to better assess 3D hydrodynamic loads on the cap and piles for different surrounding water levels and geometrical pile patterns. The scope of the paper does not address the effect of dynamic forces such as wave loads, and restricted to the assessment of the modal dynamic response of the tested bridge foundation piles in terms of vibration frequencies and modal hydrodynamic pressure distributions.

Experimental Program

Experimental Setup and Tested Specimens

A rigid brick basin illustrated in Fig. 1 was specially designed and built to carry out the dynamic tests on bridge pile foundations submerged in water. The maximum depth of the water basin is 2.65 m and its volume is divided into a lower and an upper part. The dimensions of the lower volume are 1.8 m $\times$ 1.8 m $\times$ 0.55 m and those of the upper volume are 3 m $\times$ 3 m $\times$ 2.1 m as shown in Fig. 1. The dimensions of the basin were selected the largest possible so as to simulate energy dissipation of propagating waves at infinity through significant reduction of wave reflection at the basin's rigid walls. Four reinforced stiffening columns were built to buttress each of the four lateral exterior walls against water and soil pressures. Water supply through a water pipe was also installed to control water level in the basin. The design of the reduced scale models tested in this study was inspired by a pile foundation of a continuous bridge crossing Songhua River in Northeast of China. This foundation is composed of 9 concrete piles, one concrete pile cap and one concrete pier as shown in Fig. 2. The total length of the piles is 58 m with a segment of 17.5 m above the scour line. The other dimensions of the foundation are also depicted in Fig. 2. The pier and cap were constructed using Chinese Grade C35 concrete (JTG D63-2007) having a Young's modulus of 31.5 GPa and the piles using C25 concrete having a Young's modulus of 28 GPa.

A reduced scale 9-pile foundation specimen shown in Fig. 3, with dimensions inspired from the prototype pile foundation, is built first. The specimen consists of steel tube piles, a concrete filled steel cap and a concrete pier. Bridge deck and other superstructure elements are not considered since the present work focuses on investigating the effects of fluid-structure interaction between the pile foundations and water. Steel tubes are used to simulate the concrete piles mainly because of ease of construction. They are 0.06 m in diameter and 0.001 m thick, yielding a diameter-to-thickness ratio of 60. In order to get a good pile-to-cap connection, a concrete filled steel box is used. It consists of four 0.60 m $\times$ 0.30 m $\times$ 0.05 m lateral steel plates, a 0.06 m $\times$ 0.06 m $\times$ 0.01 m steel base plate and inner cast in situ concrete. The steel used has a density of 7830 kg/m^3 and a Young's modulus of 210 GPa. The steel tube piles are welded to the base plate of the cap steel box at one end, and to another steel plate temporarily fixed to the water basin's bottom by twelve rivets. A 0.25 m thick concrete pad cast around the steel plate and tubes at the water basin's bottom so the piles of the specimens can be considered as rigidly fixed at their base. The overall dimensions of the cap are 0.6 m $\times$ 0.6 m $\times$ 0.3 m. The 1.5 m high concrete pier has a cross section of 0.2 m $\times$ 0.1 m and is reinforced with 6 Chinese Grade HRB335 (JTG D63-2007) longitudinal steel bars having a diameter of 10 mm, and HRB235 (JTG D63-2007) stirrups with a diameter of 6 mm placed at a vertical spacing of 0.1 m. The cast-in-situ concrete is designed according to Chinese Grade C15

concrete (JTG D63-2007) with a density of $2300\,\text{kg/m}^3$ and a Young's modulus of $22\,\text{GPa}$. To investigate the effects of the number and geometrical patterns of the submerged piles, the original 9-pile specimen shown in Fig. 3 is transformed into 5-pile and 4-pile specimens by removing the four side middle piles and then the central piles, respectively, as illustrated in Fig. 4.

Instrumentation and Experimental Protocol

The experimental investigation in this work involved forced vibration as well as ambient vibration tests to identify the dynamic properties of the three specimens described previously, including the natural periods as a function of different water levels. An impact steel hammer was used to excite the specimens along X and Y axes, respectively. To avoid interfering with the surrounding water: (i) the handle of the impact hammer was lengthened with a 2 meters rigid stick to excite the specimens from outside the basin, and (ii) the impact zone was located near the middle of the pier located above maximum water level as illustrated in Fig. 3.

The systems' modal dynamic response was monitored using CA-YD-103 accelerometers with a frequency range of $0.5\,\text{Hz}$ to $12\,\text{kHz}$ and with reliable waterproof protection to enable accurate signal transfert when attached on the submerged cap and piles. Fig. 5 illustrates the 12 accelerometers fixed on the pile cap, pier and piles. Data acquisition was performed using the INV306U system provided by the China Orient Institute of Noise & Vibration (China Orient Institute 2011). A sampling rate of $400\,\text{Hz}$ was used for the first chronologically tested 9-pile specimen. After post-processing of the obtained testing data, it was found that a $100\,\text{Hz}$ sampling rate was sufficient to obtain the first three modes of interest in this work. Therefore, this latter sampling rate was adopted for the forced vibration tests of the remaining 5-pile and 4-pile specimens.

In addition to forced vibration tests, ambient vibration tests were also conducted using the same instrumentation installed. For this purpose, ambient accelerations were recorded for at least three intervals of $120\,\text{sec}$ at the same sampling rate of $100\,\text{Hz}$ as previously. The ambient vibration tests were carried out to correlate the results with those from previous forced vibration tests and allow the identification of resonant frequencies that could not be excited by hammer impact.

Numerical Models

Numerical Formulation

3D finite element models of the tested bridge pile foundation specimens and surrounding water are built to compare the results to those obtained experimentally. The tested specimens are modeled using 3D solid finite elements, while the surrounding water is simulated using 3D potential-based fluid elements (PBFE). Fluid-structure interaction is accounted for through special elements at the water-cap and water-pile interfaces. The vibrations of the tested specimen cause water motions normal to its boundaries, and the induced-pressure within water cause additional hydrodynamic loads to act on the specimen. The procedure used is known as the $\phi - U$ formulation since it is expressed in terms of displacements U as

state variables in the solid domain, and velocity potentials ϕ in the fluid domain. It assumes that the fluid is inviscid, compressible or incompressible, and with an irrotational motion and relatively small displacements of the fluid-structure boundaries. Details of the $\phi - U$ formulation can be found elsewhere (Everstine 1981, Olson and Bathe 1985, Bouaanani and Lu 2009, ADINA 2010) and only a brief review is given hereafter for the sake of conciseness. Under the above assumptions, the velocity potential ϕ satisfies the wave equation

$$\nabla^2 \phi = \frac{1}{C_{\text{w}}^2} \frac{\partial^2 \phi}{\partial t^2} \tag{1}$$

where C_{w} is the velocity of compression waves within water, and t the time variable. The following boundary conditions are adopted for the velocity potential ϕ

– An essential boundary condition at the free surface and rigid four lateral walls of the water basin

$$\phi = 0 \tag{2}$$

– A natural boundary condition at the vibrating water-cap or water-pile interfaces

$$\frac{\partial \phi}{\partial n} = \dot{u}_n \tag{3}$$

where $\dot{u}_n$ denotes the positive normal velocity corresponding to unit surface normal vector $\mathbf{n}$ pointing into the water basin and out of the structure. Using standard techniques, the weak variational form of Eq. (1) can be obtained and discretized to yield the following non-standard eigenvalue problem to be solved to determine the modal response of the bridge pile foundation surrounded by water

$$\left(-\tilde{\omega}_j^2 \begin{bmatrix} \mathbf{M}_{\text{ss}} & \mathbf{0} \\ \mathbf{0} & \mathbf{M}_{\text{ff}} \end{bmatrix} - \tilde{\omega}_j \begin{bmatrix} \mathbf{0} & \mathbf{C}_{\text{fs}}^{\text{T}} \\ \mathbf{C}_{\text{fs}} & \mathbf{0} \end{bmatrix} + \begin{bmatrix} \mathbf{K}_{\text{ss}} & \mathbf{0} \\ \mathbf{0} & \mathbf{K}_{\text{ff}} \end{bmatrix} \right) \begin{bmatrix} \mathbf{U}^{(j)} \\ -\text{i}\, \mathbf{\Phi}^{(j)} \end{bmatrix} = \begin{bmatrix} \mathbf{0} \\ \mathbf{0} \end{bmatrix} \tag{4}$$

where $\text{i} = \sqrt{-1}$, $\tilde{\omega}_j$ is the coupled frequency of the bridge pile foundation-water system along mode j, $\mathbf{M}_{\text{ss}}$ and $\mathbf{K}_{\text{ss}}$ are the structural mass and stiffness matrices of the bridge pile foundation, respectively, $\mathbf{M}_{\text{ff}}$ and $\mathbf{K}_{\text{ff}}$ are the potential and kinetic energy matrices of the surrounding water, respectively, $\mathbf{C}_{\text{fs}}$ is a matrix coupling the velocity potential to displacements on the water-cap and water-pile interfaces, and $\mathbf{U}^{(j)}$ and $\mathbf{\Phi}^{(j)}$ are the modal displacement and fluid potential eigenvectors, respectively. The modal hydrodynamic pressure $p^{(j)}(x, y, z)$ for mode j at a given point of coordinates (x, y, z) of the water domain can then be obtained as

$$p^{(j)}(x, y, z) = \rho_{\text{w}}\, \omega_j\, \phi^{(j)}(x, y, z) \tag{5}$$

where ρ_{w} is the mass density of water, and $\phi^{(j)}$ is the fluid potential resulting from the interpolation of the fluid potential eigenvector $\mathbf{\Phi}^{(j)}$ at coordinates (x, y, z).

Finite Element Models

The software ADINA (2010) was used to discretize the pile foundation specimens into 20-node solid finite elements. This software implements the $\phi - U$ described previously, and was validated else-

where (Bouaanani and Lu 2009) against other analytical or classical methods for dynamic fluid-structure interaction problems in civil engineering. In this formulation, the hydrodynamic pressures developed within the potential-based fluid elements are two-way coupled to the vibrations of the solid elements modeling the bridge foundation. The 20-node potential-based finite elements programmed in ADINA (ADINA 2010) were used to model the water domain surrounding the piles. A program was developed to ensure refined meshing of the bridge foundation and surrounding water while accounting for fluid-structure interaction. The mesh densities of all the finite element models were refined until convergence of the results.

The following material properties were considered: a modulus of elasticity $E_c = 22$ GPa, a Poisson ratio $\nu_c = 0.2$, and a mass density $\rho_c = 2300$ kg/m^3 for cast-in-place concrete used to build the pier and pile cap, a modulus of elasticity $E_s = 210$ GPa, a Poisson ratio $\nu_s = 0.3$, and a mass density $\rho_s = 7830$ kg/m^3 for steel used to build the cap box and the tubular piles. Water is assumed compressible, with a velocity of compression waves $C_w = 1440$ m/s and a mass density $\rho_w = 1000$ kg/m^3.

For illustration purposes, Fig. 7 shows the finite element discretization of the 9-pile foundation specimen submerged in a full reservoir corresponding to water height $H_w = 2.05$ m. To enhance the accuracy of the numerical results, efforts were made to discretize the solid parts and fluid domain into refined brick elements with maximum side lengths of 0.05 m, and to assign mesh densities as uniformly and smoothly as possible to the different regions of the model.

For each of the 9-pile, 5-pile and 4-pile foundation specimens, finite element models of the dry structure, i.e. without water, as well as the wet structures surrounded by water reservoirs filled up to the 10 levels indicated in Fig. 6 were built. This resulted in a total number of 33 finite element models, 11 for each of the three specimens. The built finite element models were then used to run frequency-domain analyses to obtain vibration periods, modal displacements and hydrodynamic pressures.

Experimental and Numerical Results

Wet-to-dry Period Ratios

The tests were conducted considering the water levels shown in Fig. 6, corresponding to water heights H_w varying from 0 to 2.05 m for empty to full reservoir, respectively. For each water level, the first two lateral vibration modes along Y and X axes, respectively, could be excited through forced as well as ambient vibration tests, while only the latter type of tests could excite the torsional third mode around axis Z. For illustration purposes, the three mode shapes of the 9-pile foundation specimen are shown in Fig. 8. The vibration periods $\tilde{T}_j$, $j = 1 \ldots 3$, corresponding to the first three modes were determined for each water level studied. The vibration periods T_j, $j = 1 \ldots 3$, of the dry structures, i.e. without water, were also obtained experimentally. Forced vibration test results were used for the first and second lateral modes, while those from ambient vibration tests characterized the torsional third mode. The wet to dry period ratios $\tilde{T}_j/T_j$, $j = 1 \ldots 3$, were then determined to evaluate the effect of fluid-structure interaction. The results obtained are presented in Figs. 9 to 11 for the 9-pile, 5-pile and 4-pile foundation specimens, respectively, as a

function of water level ratios varying from 0 to 1 for the empty to the full reservoir, respectively. The figures also show the period ratios obtained using the finite element models described previously. It can be seen that the agreement between the experimental results and numerical predictions is very satisfactory for all the tested specimens and water level ratios. The figures also show that, as expected based on previous literature on single piles in water (Liaw and Chopra 1974), the dynamically-induced effect of fluid-structure interaction increases with water height, reaching a maximum when the reservoir is full. For the three specimens tested, we observe that higher wet to dry period ratios correspond to the two lateral modes, while lower ratios are associated with the third torsional mode. The wet to dry period ratios corresponding to the three specimens show practically the same trends, and those characterizing the 9-pile foundation specimen are slightly the highest, reaching about 1.06 for the two lateral modes, and 1.04 for the torsional mode, both occurring when reservoir is full. The curves also reveal that the vibration period of the system remains practically constant for water level ratios up to 0.5, and that period lengthening due to fluid-structure interaction becomes more noticeable for larger water heights, with a steep increase observed between water level ratios of 0.8 and 1.0. This behavior can be explained by the fact that hydrodynamic effects become predominant as the area of involved fluid-structure interfaces increases. This is the case for water level ratios larger than 0.8, corresponding to fluid-structure interaction through the lateral faces of the pile cap, characterized by an area much larger than that associated to fluid-structure interaction with the piles below. Following the same analysis, the surfaces involved in fluid-structure interaction around the piles of the three specimens are different, which explains the slight differences between the wet to dry period ratios corresponding to water level ratios less than 0.8. It is important to note that the previous results focused on the analysis of the tested cantilevered bridge foundations, where only the first three translational and torsional modes are the most significant in the dynamic response. However, the validated numerical models could be eventually used to extend the analyses to cases of other types of bridge foundations characterized by a more important contribution of higher modes.

Hydrodynamic Pressures

In this section, we investigate further the effect of fluid-structure interaction on the response of the tested specimens through the analysis of induced modal hydrodynamic pressures. For this purpose, the finite element models described previously and validated against experimental data are used. The absolute values of modal hydrodynamic pressures corresponding to the first three modes were computed using finite elements to illustrate the 3D distribution of hydrodynamic loads as a function of pile patterns and water levels. For clarity, the obtained hydrodynamic pressures are illustrated for each mode through 2D contour maps along vertical and horizontal cutting planes selected as a function of pile pattern and water level. The hydrodynamic pressures are nondimensionalized through scaling by the maximum hydrostatic pressure $p_{\text{stat}} = \rho_{\text{w}} \text{g} H_{\text{w}}$ to facilitate comparison between the different cases. For brevity, only results for the first lateral and third torsional modes and two water levels are illustrated next. The nondimensionalized hydrodynamic pressures for the first lateral mode of the 9-pile foundation specimen surrounded by a full reservoir at $H_{\text{w}} = 2.05\,\text{m}$ are shown in Figs. 12 (a) to (d), corresponding, respectively, to a vertical cutting plane $x = -0.15\,\text{m}$ passing through the middle of the row of three exterior piles, a vertical

cutting plane $x = 0$ m passing through the middle of the central row of three piles, a horizontal cutting plane $z = 1.90$ m passing through the middle of the pile cap, and a horizontal cutting plane $z = 1.35$ m. Figs. 12 (e) to (h) illustrate the nondimensionalized hydrodynamic pressures corresponding to the torsional third mode of the 9-pile foundation specimen surrounded by a full reservoir at $H_{\text{w}} = 2.05$ m and along the same cutting planes described previously. It can be seen that higher hydrodynamic pressures are mainly concentrated around the cap structure, approximately at the middle horizontal cutting plane, i.e. Figs. 12 (a) and (e). The horizontal cutting plane views, i.e. Figs. 12 (c) and (g), show that the high pressures occur at the middle of the cap lateral faces for lateral modes, and near the cap corners for the torsional mode. Hydrodynamic pressures in the latter case are the largest, a result that can be explained by the more important fluid-structure interface area involved during torsional modes compared to the lateral modes. The hydrodynamic pressures exerted on the piles are lower in comparison with those on the cap, with maximum values occurring at the four corner piles along the torsional mode, i.e. Fig. 12 (h). Figs. 12 (a), (b) and (d) reveal that hydrodynamic pressures corresponding to the lateral modes are larger on external piles. These figures also show that hydrodynamic loads on the central pile are practically null.

The nondimensionalized hydrodynamic pressures corresponding to the lateral and torsional modes of the 5-pile and 4-pile foundation specimens surrounded by a full reservoir at $H_{\text{w}} = 2.05$ m and along the same cutting planes described previously are presented in Figs. 13 and 14, respectively. As for the 9-pile foundation specimen, we observe that larger hydrodynamic pressures occur mainly around the cap structure and approximately at the same locations, and that the torsional mode induce higher hydrodynamic loads than the lateral modes. Also as previously, the piles are subjected to lower hydrodynamic pressures than the cap, with maximum loads around the four corner piles along the torsional mode. We deduce from the comparison of Figs. 12 to 14 that hydrodynamic pressures become globally lower as the number of piles diminishes from 9 to 4 which corresponds to decreasing structural stiffness of the pile foundation system and increasing spacing between the piles. Figs. 12 to 14 also show that rigid wall boundary conditions of the used water basin do not have a significant influence on the distribution of hydrodynamic pressure around the piers for the considered modes of vibration. This result supports the dimensions of the water basin used for the tests were sufficiently large to simulate energy dissipation of propagating waves far from the pile foundations.

Figs. 15 to 17 illustrate the hydrodynamic pressures on the 9-pile, 5-pile and 4-pile foundation systems considering a water height of $H_{\text{w}} = 1.75$ m, corresponding to the bottom of the pile cap. The contour maps of nondimentionalized hydrodynamic pressures are shown along the same cutting planes defined previously, except the horizontal cutting plane $z = 1.90$ m now replaced by plane $z = 1.75$ m located at the same level as the bottom of the cap. The results show that hydrodynamic loads are lower than for the full reservoir case discussed previously. The vertical profiles of hydrodynamic pressures are now more distributed along pile lengths and differ from the previous cases, for example Fig. 12 (a) vs. Fig. 15 (a) or Fig. 12 (b) vs. Fig. 15 (b). Large hydrodynamic pressures occur around the external piles with the highest values corresponding to the torsional mode. Again, hydrodynamic pressures globally decrease as the number of piles diminishes from 9 to 4 due to structural stiffness reduction and higher spacing between

the piles.

Summary and Conclusions

This paper described an experimental program conducted to investigate the effects of fluid-structure interaction on the modal dynamic response of three reduced-scale bridge pile foundations submerged partially or totally in water. The three specimens built differ by the number of piles, i.e. 9, 5 and 4, and their geometrical patterns. The results of the ambient and forced-vibration tests were presented and discussed as a function of surrounding water levels and the number and geometrical patterns of the piles. Considering that the evaluation of vibration periods of deep water bridges are crucial for their seismic design or safety evaluation under earthquake excitation, these parameters were measured for the two lateral modes and first torsional mode of the tested wet structures, i.e. including water effects, to assess the effect of fluid-structure interaction. Wet-to-dry period ratios were then determined as a function of water height and numerical and geometrical patterns of the piles. Three-dimensional (3D) finite element models of the tested specimens were built and the results were validated against the obtained experimental data. A very satisfactory agreement was obtained between the experimental and numerical results. The modal hydrodynamic pressures were then computed using the validated models to illustrate the 3D distribution of hydrodynamic loads as a function of pile patterns and water levels.

The findings obtained through a comprehensive analysis of the period ratios and hydrodynamic pressures mainly showed that: (i) the effect of fluid-structure interaction on grouped piles increases with water height, a result that was also observed for single pile or tower structures in previous research; (ii) the variation of wet-to-dry period ratios as a function of water height show practically the same trend for each mode of vibration of all the tested specimens, (iii) the wet-to-dry period ratios corresponding to the two lateral modes are higher than those associated with the torsional mode; (iv) the hydrodynamic pressures are mainly concentrated around the cap structure, with maximum values corresponding to the torsional mode. This work also emphasized that period lengthening due to fluid-structure interaction becomes more noticeable when the pile cap is also submerged into water. The hydrodynamic pressures were shown to become globally lower as the number of piles diminishes from 9 to 4, a behavior that can be related to the combined effects of decreasing structural stiffness and the larger spacing between the piles. It is important to note that the conclusions of this work should be considered in the context of the experimental tests conducted and that they cannot be directly extrapolated to real bridge cases involving additional effects of superstructure and water wave loads. However, the observed complex distributions of hydrodynamic loads may significantly affect the seismic structural response and should be assessed adequately during the design and construction of deep water pile foundations similar to those studied. Overall, the experimental and numerical results of this research allow a better understanding of the dynamically-induced fluid-structure interaction effects in the response of deep water bridge pile foundations, and set the basis for comprehensive 3D finite element analyses of large scale bridge structures of the same type.

Acknowledgements

This research was supported by the National Nature Science Foundation of China (Grants No. 50978194 and 90915011), the Kwang-Hua Fund for College of Civil Engineering and the Ph.D. Short-term Academic Visiting Fund of Tongji University, Shanghai, China. The authors would also like to thank Prof. Qiwei Zhang, Mr. Yongji Wu and Mr. Yutao Pang of the Department of Bridge Engineering, Tongji University and Prof. Chih-Chen Chang of the Department of Civil and Environmental Engineering, Hong Kong University of Science and Technology, for their help in preparing the experiments.

References

AbdelSalam, S. S., Sritharan, S., and Suleiman, M. T. (2010). "Current design and construction practices of bridge pile foundations with emphasis on implementation of LRFD." *J. Bridge Eng.*, 15(6), 749-758.

ADINA. (2010). "Theory and modeling guide." *Rep. ARD 10-7, ADINA R&D, Inc.*, Watertown, MA.

Bhatta, D. D., and Rahman, M. (2003). "On scattering and radiation problem for a cylinder in water of finite depth." *Int. J. Eng. Sci.*, 41(9), 931-967.

Bittner, R. B., Zhang, X. G., and Jensen, O. J. (2007). "Design and construction of the Sutong Bridge foundations." *DFI J.*, 1(1), 1-18.

Bouaanani, N., and Lu, F. Y. (2009). "Assessment of potential-based fluid finite elements for seismic analysis of dam¨Creservoir systems." *Comput. Struct.*, 87(3-4), 206-224.

China Orient Institute of Noise & Vibration, http://www.coinv.com/en/, Date accessed: October 2011.

Ministry of Communications of China. (2007). *Code for design of ground base and foundation of highway bridges and culverts*. JTG D63-2007, Beijing, China (In Chinese).

DiMaggio, J. A., and Goble, G. G. (2004). "Developments in deep foundation highway practice – The last quarter century." *ASCE Con. Proc.*, Los Angeles, California, USA, 110-127.

Di Pilato, M., Perotti, F., and Fogazzi, P. (2008). "3D dynamic response of submerged floating tunnels under seismic and hydrodynamic excitation." *Eng. Struct.*, 30(1), 268-281.

Everstine, G. C. (1981). "A symmetric potential formulation for fluid-structure interaction." *J. Sound Vib.*, 79(1), 157-160.

Feng, M. (2009). "China's Major Bridges." *IABSE Symposium Report*, Shanghai, China, 1-24.

Gao, Y., Yuan, W. C., and Jin, X. G. (2008). "Soil-structure-water ineraction of a cable-stayed bridge under seismic excitation." *Proc., 14th World Conf. on Earthquake Eng.*, Beijing, China.

Ingham, T. J., Rodriguez, S., Donikian, R. and Chan, J. (1999). "Seismic analysis of bridges with pile foundations." *Comput. Struct.*, 72(1-3), 49-62

Liaw, C. Y., Chopra, A. K. (1973). "Earthquake response of axisymmetric tower structures surrounded by water." *Rep. No. UCB/EERC-73/25*, Univ. of California, Berkeley, Berkeley, Calif.

Liaw, C. Y., and Chopra, A. K. (1974). "Dynamics of towers surrounded by water." *Earthq. Eng. Struct. D.*, 3(1), 33-49.

Liu, S. X., Li, Y. C. and Li, G. W. (2007). "Wave current forces on the pile group of base foundation for the east sea bridge, China." *J. Hydrodyn.*, 19(6), 661-670.

Morison, J. R., O'Brien, M. P., Johnson, J. W., and Schaaf, S. A. (1950). "The force exerted by surface waves on piles." *Petrol. T.*, 189, 149-154.

Olson, L. G., and Bathe, K. J. (1985). "An infinite element for analysis of transient fluid-structure interactions." *Eng. Computation.*, 2(4), 319-329.

Öz H. R. (2003). "Natural frequencies of an immersed beam carrying a tip mass with rotatory inertia." *J. Sound Vib.*, 266(5), 1099-1108.

Uściłowska, A., and Kołodziej, J. A. (1998). "Free vibration of immersed column carrying a tip mass." *J. Sound Vib.*, 216(1), 147-157.

Virola, J. (2005). "A review of long-span suspension bridges: a case of Akashi-Kaikyo and Runyang south bridges." *Botswana J. Technol.*, 14(1), 43-50.

Wei, K., Wu, Y. J., Pang, Y. T., Xu, C., and Yuan, W. C. (2011). "Numerical dynamic analysis for water-pile group bridge foundation interacted system." *Gongcheng Lixue*, 28(SUPPL. 1), 195-200 (In Chinese).

You, Q. Z., He, P., Dong, X. W., Zhang, X. G., and Wu, S. C. (2008). "Sutong bridge - The longest cable-stayed bridge in the world." *J. SEI - IABSE*, 18(4), 390-395.

Zhang, C. H. (2001). *Numerical modelling of concrete dam-foundation-reservoir systems*, Tsinghua University Press, Beijing, China.

Zhang, M. (2006). "Vibration analysis of solid-fluid interaction for the pier-river water." M.E. thesis, Dalian Jiaotong Univ., Dalian, China

List of figures

Fig. 1: Dimensions of the rigid brick basin used for the dynamic tests.

Fig. 2: Dimensions of the prototype pile foundation which inspired the geometry of the specimens tested.

Fig. 3: Dimensions and details of the reduced 9-pile foundation specimen tested dynamically.

Fig. 4: Patterns of the piles of the two other tested specimens.

Fig. 5: Experimental setup: (a) Positions of the 12 accelerometers fixed on the cap, pier and piles of the tested specimens, and (b) Global view of the specimen and testing setup.

Fig. 6: Water levels used during the tests.

Fig. 7: Finite element model of the 9-pile foundation specimen and surrounding water.

Fig. 8: First three mode shapes of the 9-pile foundation specimen without water.

Fig. 9: Measured and computed wet to dry period ratios for the 9-pile foundation specimen as a function of water level.

Fig. 10: Measured and computed wet to dry period ratios for the 5-pile foundation specimen as a function of water level.

Fig. 11: Measured and computed wet to dry period ratios for the 4-pile foundation specimen as a function of water level.

Fig. 12: Nondimensional modal hydrodynamic pressures on the 9-pile foundation specimen for a water level $H_{\mathrm{w}} = 2.05$ m.

Fig. 13: Nondimensional modal hydrodynamic pressures on the 5-pile foundation specimen for a water level $H_{\mathrm{w}} = 2.05$ m.

Fig. 14: Nondimensional modal hydrodynamic pressures on the 4-pile foundation specimen for a water level $H_{\mathrm{w}} = 2.05$ m.

Fig. 15: Nondimensional modal hydrodynamic pressures on the 9-pile foundation specimen for a water level $H_{\mathrm{w}} = 1.75$ m.

Fig. 16: Nondimensional modal hydrodynamic pressures on the 5-pile foundation specimen for a water level $H_{\mathrm{w}} = 1.75$ m.

Fig. 17: Nondimensional modal hydrodynamic pressures on the 4-pile foundation specimen for a water level $H_{\mathrm{w}} = 1.75$ m.

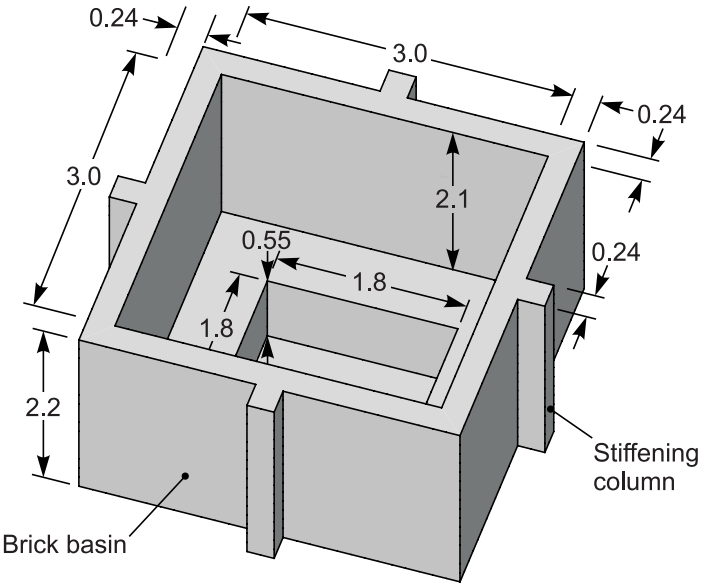

Figure 1. Dimensions of the rigid brick basin used for the dynamic tests (All dimensions are in meters).

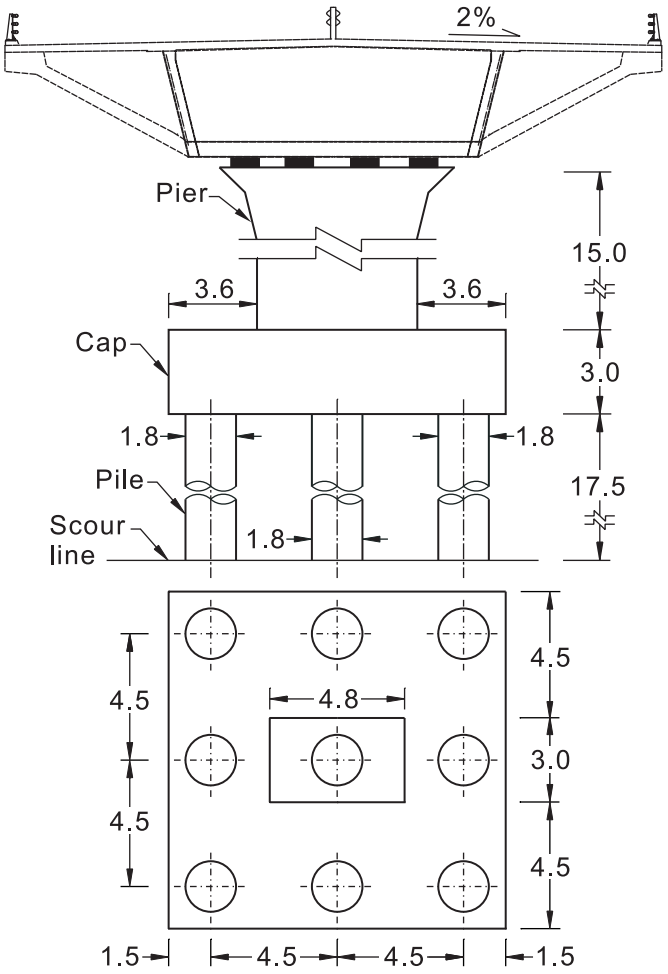

Figure 2. Dimensions of the prototype pile foundation which inspired the geometry of the specimens tested (All dimensions are in meters).

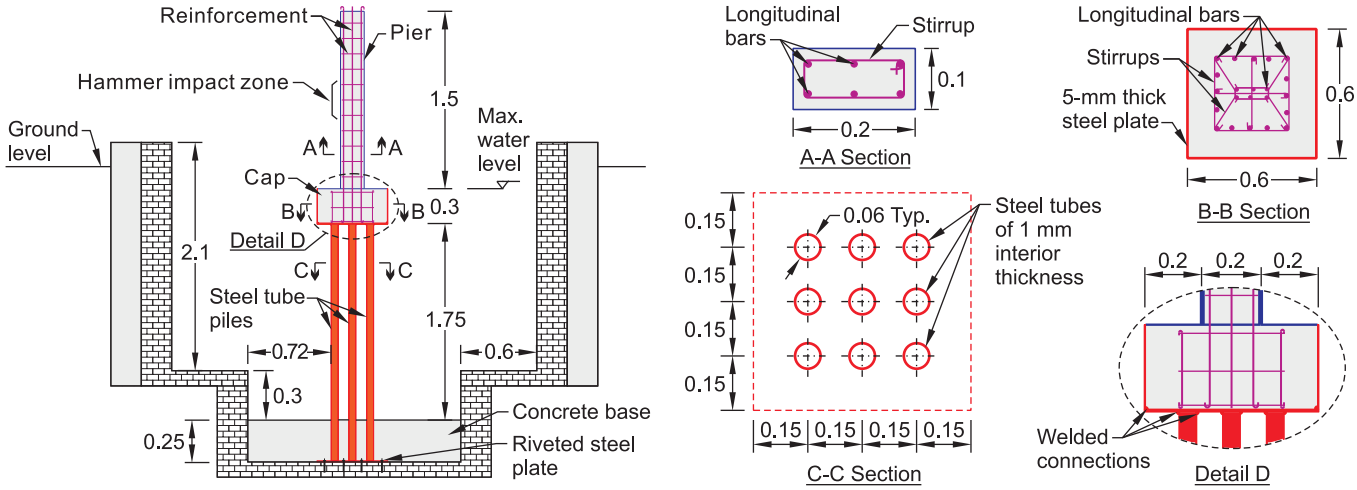

Figure 3. Dimensions and details of the reduced 9-pile foundation specimen tested dynamically (All dimensions are in meters unless otherwise specified).

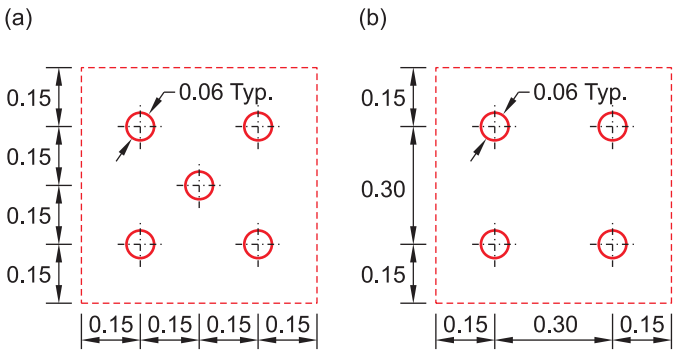

Figure 4. Patterns of the piles of the two other tested specimens: (a) 5-pile foundation specimen, and (b) 4-pile foundation specimen (All dimensions are in meters).

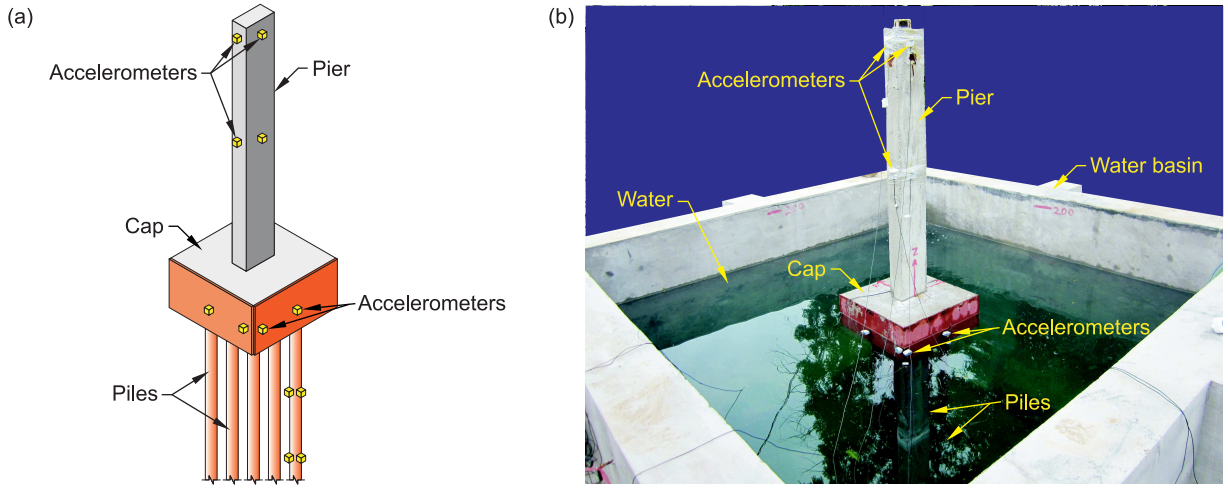

Figure 5. Experimental setup: (a) Positions of the 12 accelerometers fixed on the cap, pier and piles of the tested specimens, and (b) Global view of the specimen and testing setup.

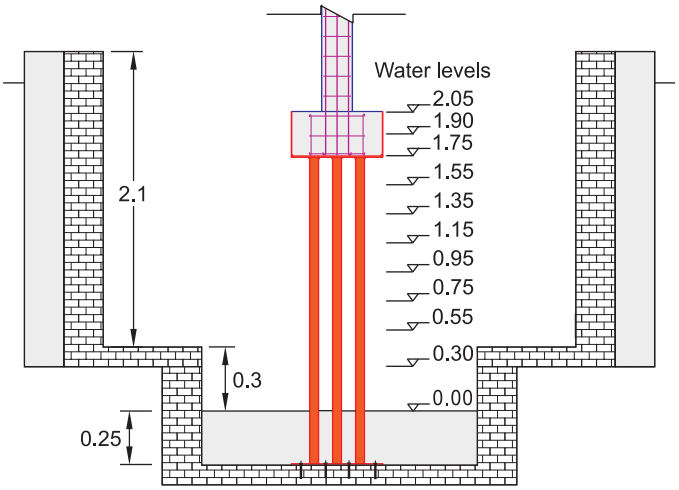

Figure 6. Water levels used during the tests (All dimensions are in meters).

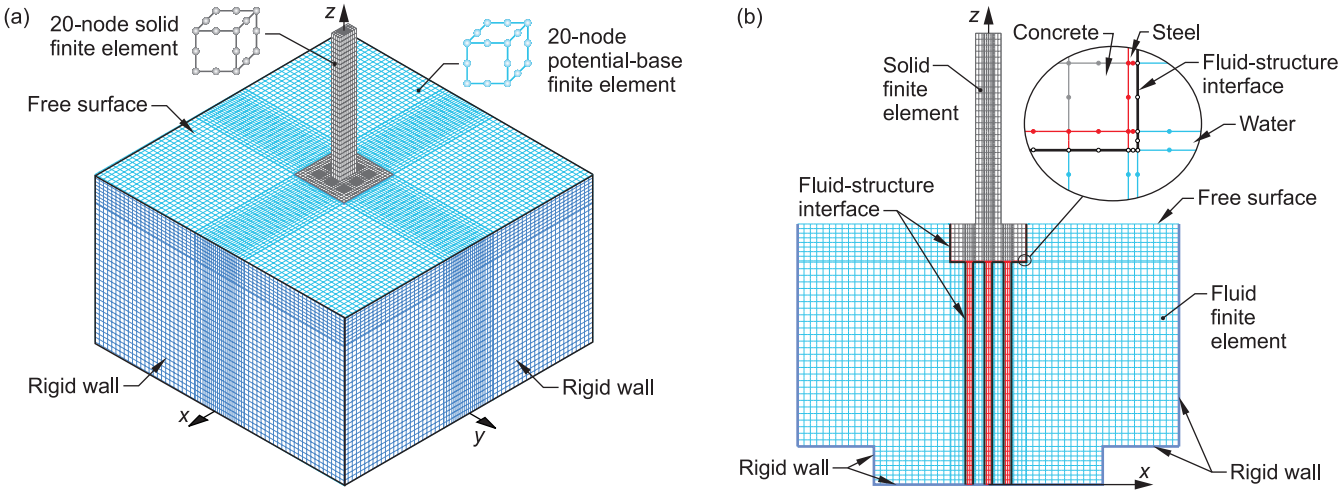

Figure 7. Finite element model of the 9-pile foundation specimen and surrounding water: (a) 3D view, (b) 2D elevation through a central cutting plane.

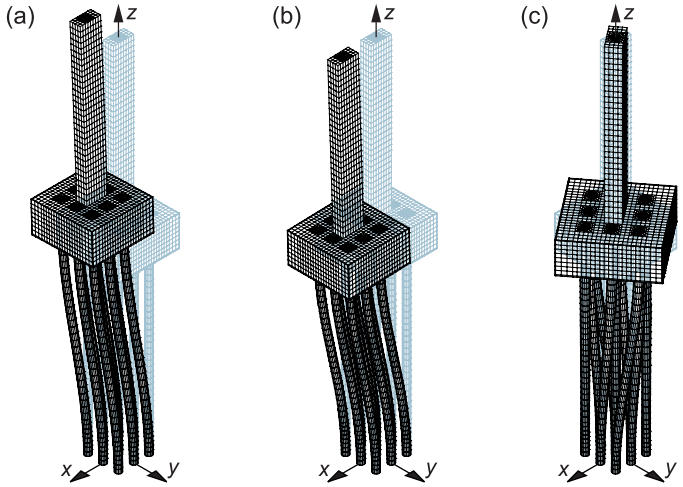

Figure 8. First three mode shapes of the 9-pile foundation specimen without water: (a) First lateral mode, (b) Second lateral mode, (c) Torsional mode.

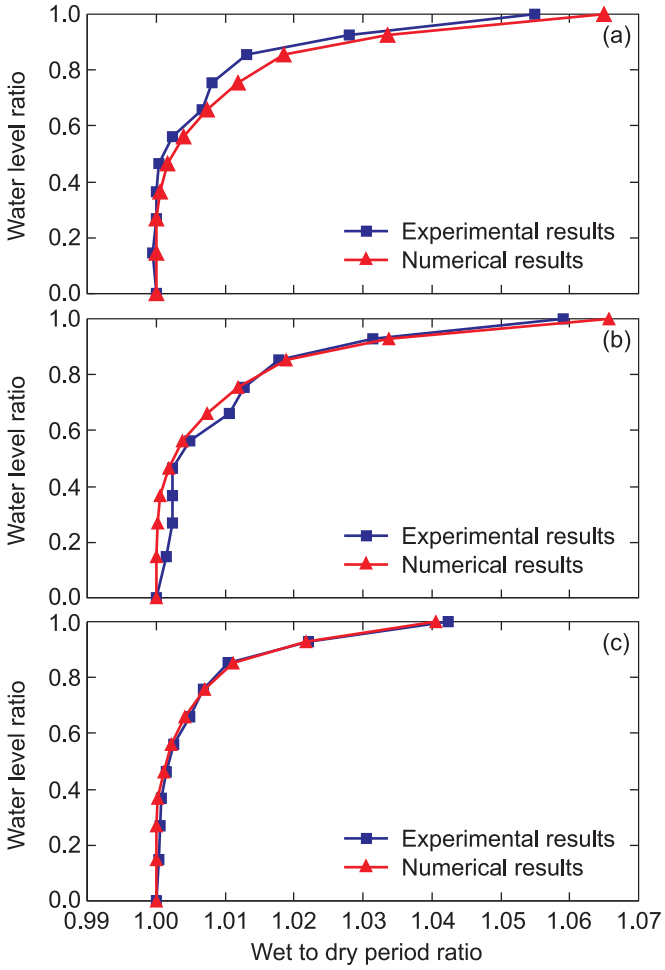

Figure 9. Measured and computed wet to dry period ratios for the 9-pile foundation specimen as a function of water level: (a) First lateral vibration mode, (b) Second lateral vibration mode, (c) Torsional mode.

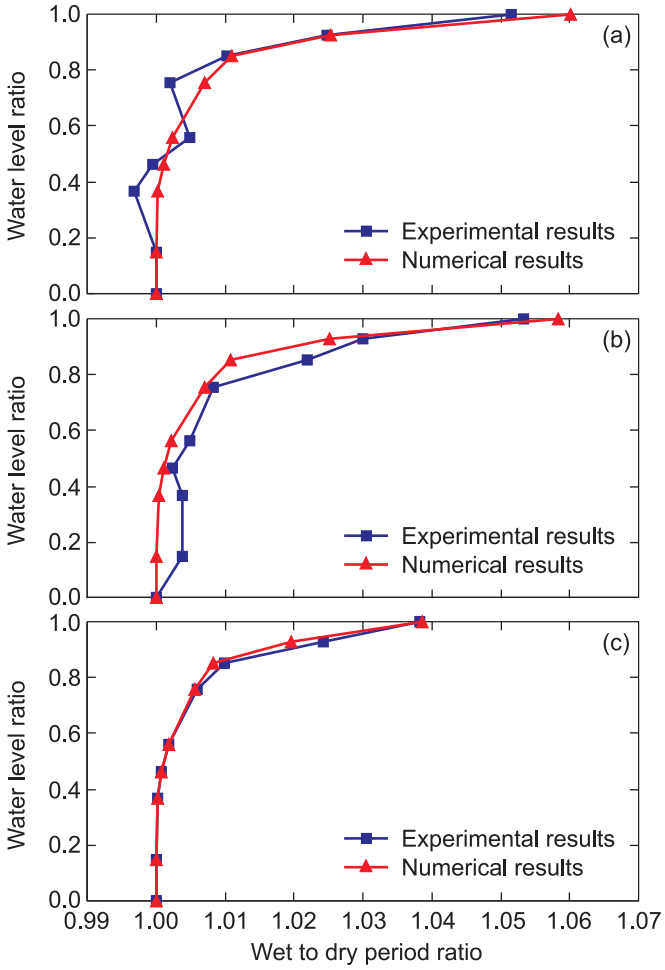

Figure 10. Measured and computed wet to dry period ratios for the 5-pile foundation specimen as a function of water level: (a) First lateral vibration mode, (b) Second lateral vibration mode, (c) Torsional mode.

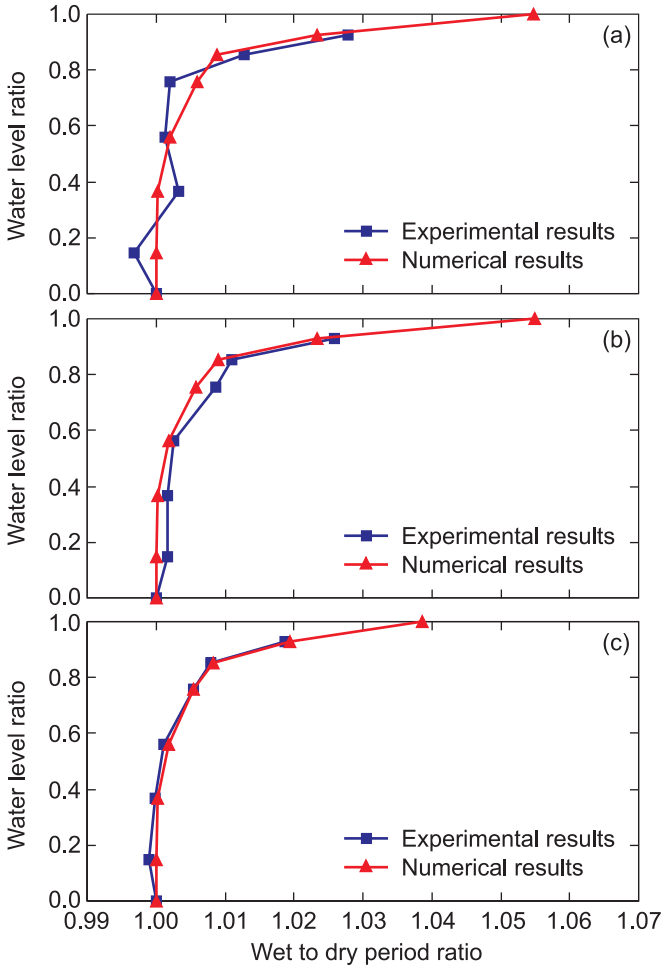

Figure 11. Measured and computed wet to dry period ratios for the 4-pile foundation specimen as a function of water level: (a) First lateral vibration mode, (b) Second lateral vibration mode, (c) Torsional mode.

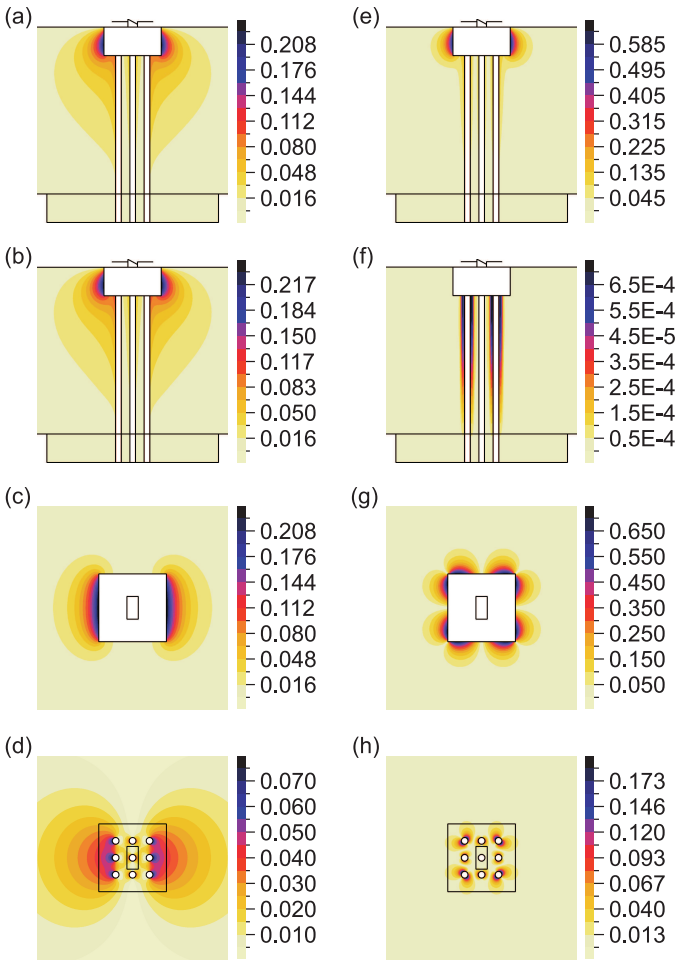

Figure 12. Nondimensional modal hydrodynamic pressures on the 9-pile foundation specimen for a water level $H_{\mathrm{w}} = 2.05\,\mathrm{m}$: (a) to (d) First lateral mode along cutting planes $x = -0.15\,\mathrm{m}$, $x = 0\,\mathrm{m}$, $z = 1.90\,\mathrm{m}$ and $z = 1.35\,\mathrm{m}$, respectively; (e) to (f) Torsional mode along cutting planes $x = -0.15\,\mathrm{m}$, $x = 0\,\mathrm{m}$, $z = 1.90\,\mathrm{m}$ and $z = 1.35\,\mathrm{m}$, respectively.

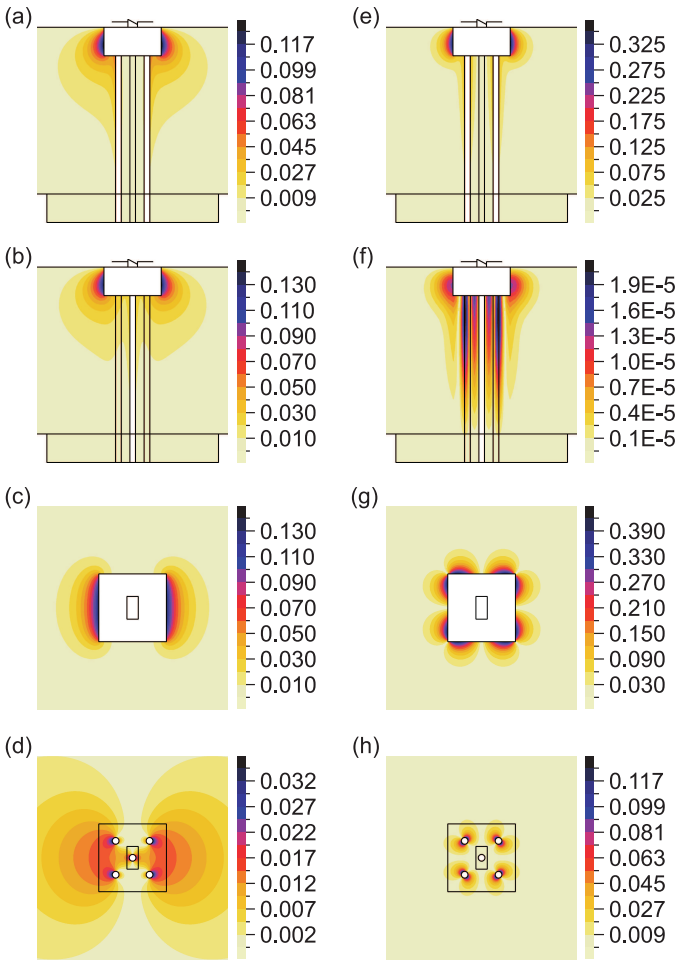

Figure 13. Nondimensional modal hydrodynamic pressures on the 5-pile foundation specimen for a water level $H_{\mathrm{w}} = 2.05\,\mathrm{m}$: (a) to (d) First lateral mode along cutting planes $x = -0.15\,\mathrm{m}$, $x = 0\,\mathrm{m}$, $z = 1.90\,\mathrm{m}$ and $z = 1.35\,\mathrm{m}$, respectively; (e) to (f) Torsional mode along cutting planes $x = -0.15\,\mathrm{m}$, $x = 0\,\mathrm{m}$, $z = 1.90\,\mathrm{m}$ and $z = 1.35\,\mathrm{m}$, respectively.

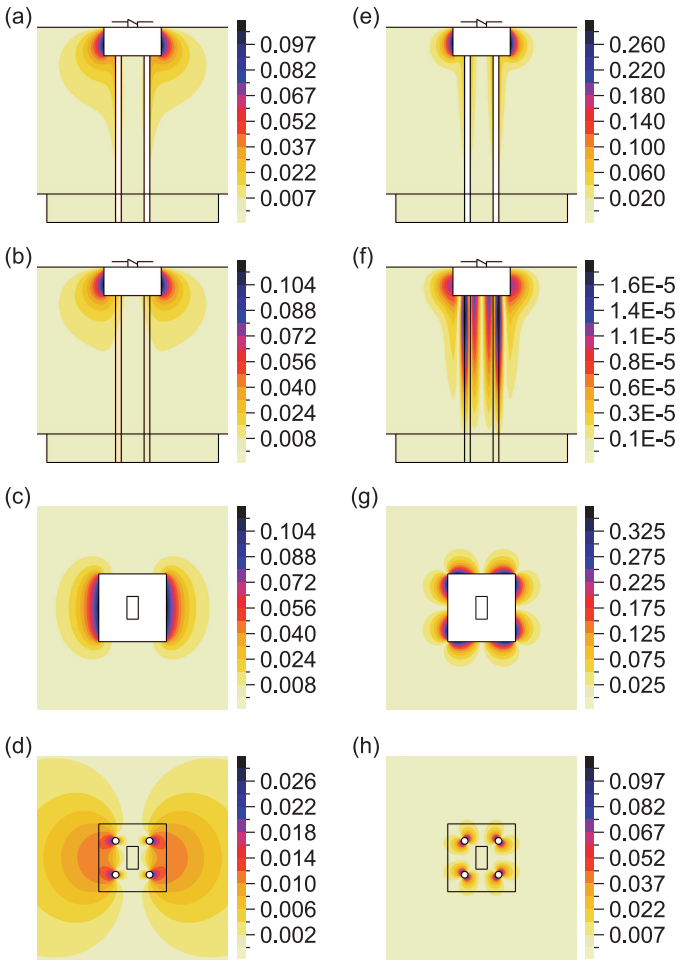

Figure 14. Nondimensional modal hydrodynamic pressures on the 4-pile foundation specimen for a water level $H_{\mathrm{w}} = 2.05\,\mathrm{m}$: (a) to (d) First lateral mode along cutting planes $x = -0.15\,\mathrm{m}$, $x = 0\,\mathrm{m}$, $z = 1.90\,\mathrm{m}$ and $z = 1.35\,\mathrm{m}$, respectively; (e) to (f) Torsional mode along cutting planes $x = -0.15\,\mathrm{m}$, $x = 0\,\mathrm{m}$, $z = 1.90\,\mathrm{m}$ and $z = 1.35\,\mathrm{m}$, respectively.

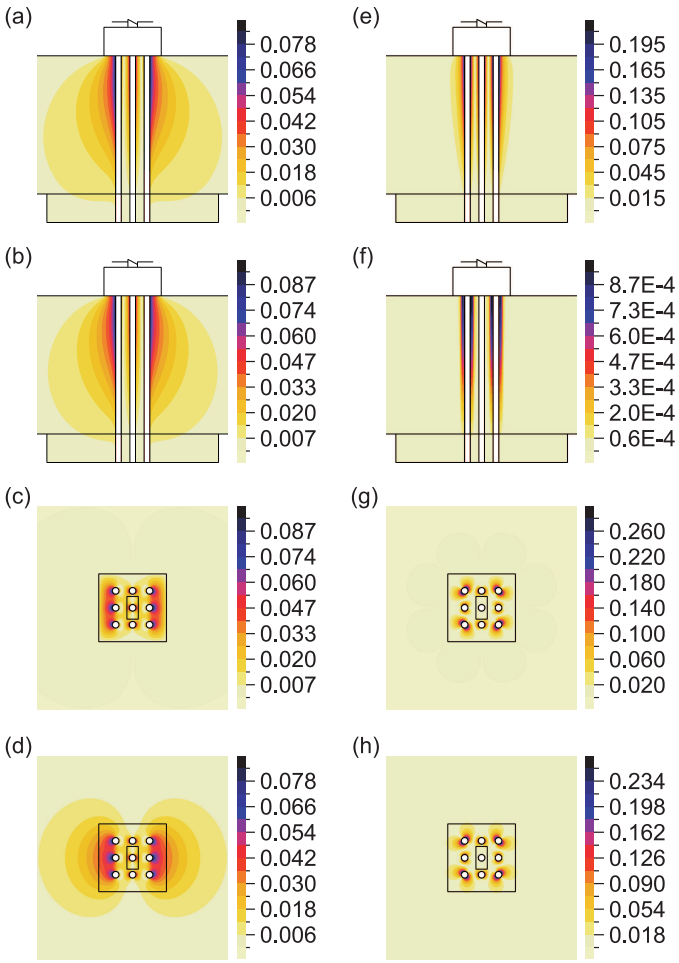

Figure 15. Nondimensional modal hydrodynamic pressures on the 9-pile foundation specimen for a water level $H_{\mathrm{w}} = 1.75\,\mathrm{m}$: (a) to (d) First lateral mode along cutting planes $x = -0.15\,\mathrm{m}$, $x = 0\,\mathrm{m}$, $z = 1.75\,\mathrm{m}$ and $z = 1.35\,\mathrm{m}$, respectively; (e) to (f) Torsional mode along cutting planes $x = -0.15\,\mathrm{m}$, $x = 0\,\mathrm{m}$, $z = 1.75\,\mathrm{m}$ and $z = 1.35\,\mathrm{m}$, respectively.

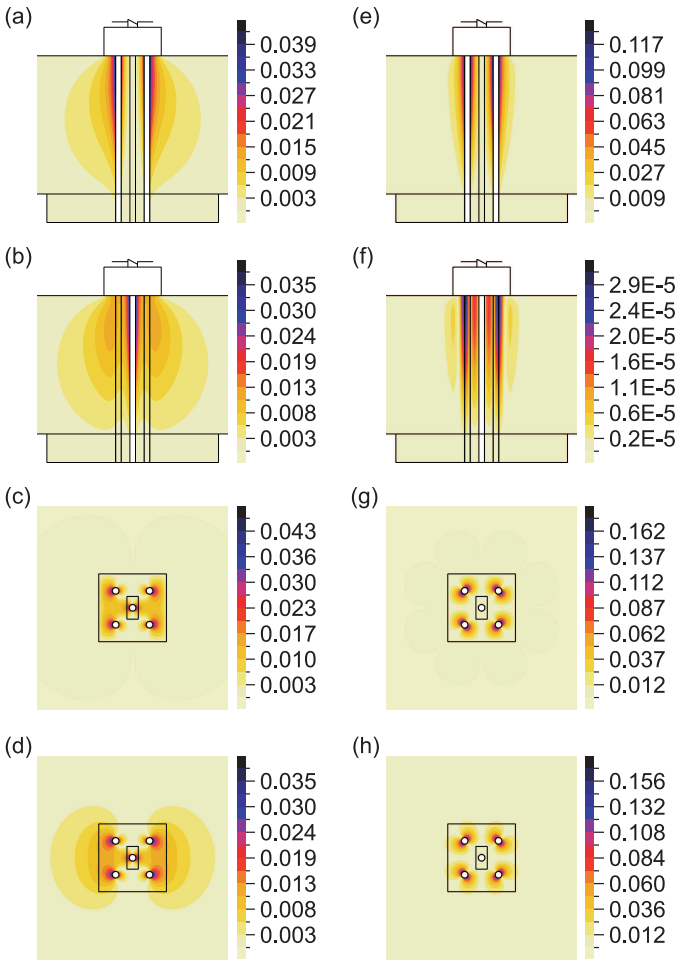

Figure 16. Nondimensional modal hydrodynamic pressures on the 5-pile foundation specimen for a water level $H_{\mathrm{w}} = 1.75\,\mathrm{m}$: (a) to (d) First lateral mode along cutting planes $x = -0.15\,\mathrm{m}$, $x = 0\,\mathrm{m}$, $z = 1.75\,\mathrm{m}$ and $z = 1.35\,\mathrm{m}$, respectively; (e) to (f) Torsional mode along cutting planes $x = -0.15\,\mathrm{m}$, $x = 0\,\mathrm{m}$, $z = 1.75\,\mathrm{m}$ and $z = 1.35\,\mathrm{m}$, respectively.

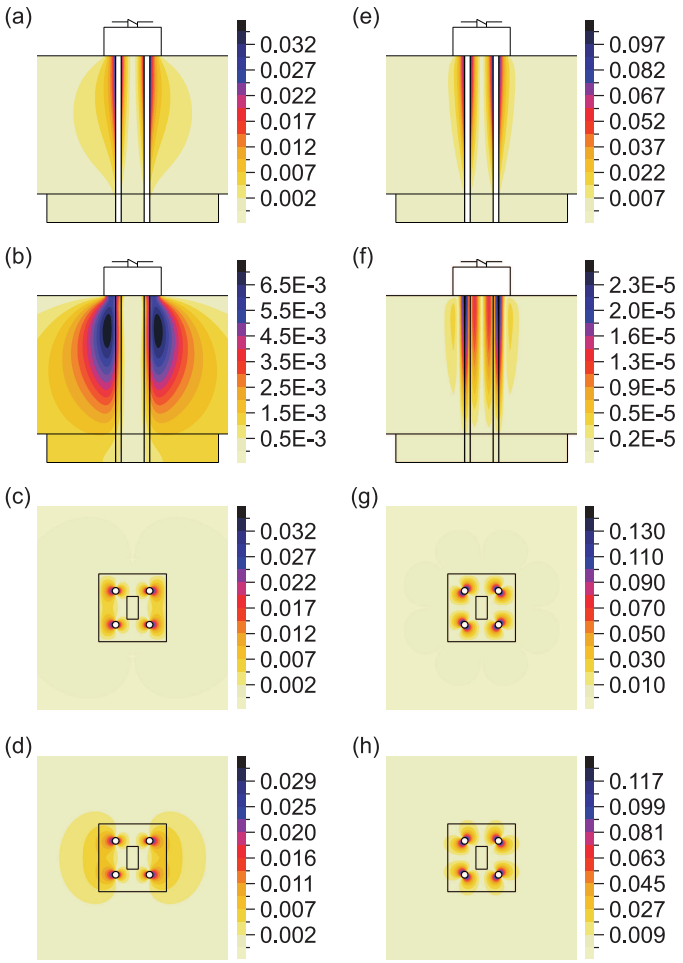

Figure 17. Nondimensional modal hydrodynamic pressures on the 4-pile foundation specimen for a water level $H_{\mathrm{w}} = 1.75\,\mathrm{m}$: (a) to (d) First lateral mode along cutting planes $x = -0.15\,\mathrm{m}$, $x = 0\,\mathrm{m}$, $z = 1.75\,\mathrm{m}$ and $z = 1.35\,\mathrm{m}$, respectively; (e) to (f) Torsional mode along cutting planes $x = -0.15\,\mathrm{m}$, $x = 0\,\mathrm{m}$, $z = 1.75\,\mathrm{m}$ and $z = 1.35\,\mathrm{m}$, respectively.